Encapsulation Residual Stress and Ferrite Loss in Inductive Coil Assemblies

Andrew Foote[1,2], Daniel Costinett[2,4], William Henken[1,2], Ruediger Kusch[3], Mostak Mohammad[4], Omer Onar[4]
[1]Innovation Hub Knoxville, Volkswagen Group of America, Knoxville, TN, USA
[2]The University of Tennessee-Knoxville, Knoxville, TN, USA
[3]Volkswagen Group Components, Volkswagen Group AG, Wolfsburg, Germany
[4]Vehicle Power Electronics Research Group, Oak Ridge National Laboratory, Oak Ridge, TN, USA
Email: afoote5@vols.utk.edu

2023 IEEE Energy Conversion Congress and Exposition (ECCE) | 979-8-3503-1644-5/23/$31.00 ©2023 IEEE | DOI: 10.1109/ECCE53617.2023.10362318

***Abstract*—As inductive wireless charging reaches higher power levels, thermal management and mechanical durability become more critical. To address these concerns, past works have demonstrated the benefit of encapsulating coil assemblies in thermally conductive materials. However, due to the sensitivity of the MnZn ferrites commonly used in coil assemblies to mechanical stress, care must be taken to avoid creating large stresses in the ferrite that cause higher hysteresis loss. The stress formation in the encapsulant curing process is overviewed and modeled and an experiment is performed to demonstrate the effect in a small-scale coil assembly. Finally, the effect is shown in the reduced coil-coil efficiency of a first generation high power inductive power transfer prototype using a stiff epoxy compared to better performance in a second prototype using a softer thermally-conductive silicone encapsulant.**

***Index Terms*—wireless power transfer, inductive power transmission, coil design, compressive stress, encapsulation, magnetic materials**

I. Introduction

INDUCTIVE power transfer (IPT) continues to mature in electric vehicle and bus charging. As IPT reaches higher power levels in smaller footprints, mechanical and thermal requirements become primary concerns. As the power level of the IPT systems increase, so do the losses in the power electronics, conductors, and magnetic materials. If these losses are not effectively dissipated through active or passive cooling, the temperatures of components of the WPT system will increase. If temperatures exceed the limits of the materials, such as the temperature ratings of semiconductor switches, wire insulation, or enclosure materials, the system operation can be compromised. Below these ultimate limits, other thermal effects such as thermal cycling stress and increases in conductor resistance must be considered for their impact on reliability and efficiency.

Several works [2, 3] have considered the introduction of encapsulants for the coil conductors and shielding magnetic materials, which, for the 85 kHz frequency band, are usually Manganese-Zinc (MnZn) ferrite tiles backed by aluminum as in Fig. 2c. The encapsulation of the conductors and ferrite can help reduce hotspots in the assembly, reduce thermal resistance for cooling, and provide robust mechanical support. A large variety of materials used for encapsulating electronic components and motors are available [4]. However, due to high alternating electric and magnetic fields within the coil area, the encapsulants used in the coil assemblies are chosen to be electrically nonconductive and nonmagnetic while having high thermal conductivity. In terms of mechanical properties, high tensile strength and adhesion are preferable in the ground assembly (GA) and especially in the vehicle assembly (VA) where the ferrite and wire are supported and protected by the encapsulant from shock, impact, and vibration. The temperature rating of the encapsulant must also be high as the wire and ferrite may range from 50°C to over 100°C during operation [2, 3]. To meet these mechanical and thermal requirements, some works [3] have used a durable, hard encapsulating material such as an epoxy resin with thermally conductive fillers. However, the residual

Parts of this work are published in a dissertation [1].

This work was funded by Volkswagen Group Innovation in collaboration with the CURENT Engineering Research Center at the University of Tennessee, Knoxville and the Power Electronics and Electric Machinery Research Center at Oak Ridge National Laboratory.

This work made use of the Engineering Research Center Shared Facilities supported by the Engineering Research Center Program of the National Science Foundation and DOE under NSF Award Number EEC-1041877 and the CURENT Industry Partnership Program. Any opinions, findings and conclusions or recommendations expressed in this material are those of the authors and do not necessarily reflect those of the National Science Foundation.

Table I
THERMO-MECHANICAL PROPERTIES OF ENCAPSULANTS AND COIL MATERIALS

	Aremco-Bond 2315	Cooltherm SC-320	MnZn Ferrite [8]	Alum. 6061-T6
Thermal Conductivity (W/mK)	1.2	3.0	3.5	167
Thermal Expansion (10^{-6}/K)	34	110	10	23.6
Young's Modulus (Shore Hardness)	4.2 GPa (92D)	3.1 MPa (54A)	90-150 GPa	69 GPa
Ultimate Tensile Strength (MPa)	84.8	2.16	20-65	310
Cure Shrinkage	0.3%	N/A	N/A	N/A
Curing Cycle	120°C/ 6 hours	25°C/ 24 hours 125°C/ 1 hour	N/A	N/A

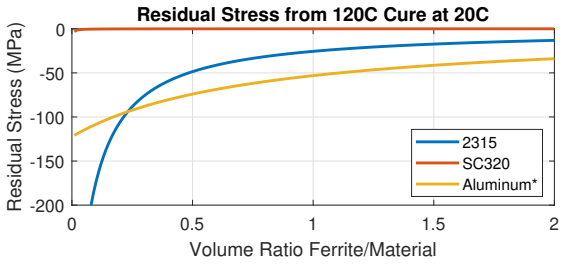

Fig. 1. Compressive stress at 20°C on ferrite from a 120°C cure as a function of the volume ratio of ferrite to the encasing material, including cure shrinkage and thermal expansion. *Aluminum only adds significant stress on the ferrite with encapsulants with high adhesive strength and hardness.

stress caused by thermal expansion, cure shrinkage, and high hardness or Young's moduli must be considered to prevent unwanted stresses on the ferrite. Avoiding cracks in the brittle ferrite is important alone [5], but the effect of stress on the magnetic performance of the ferrite must also be considered.

Placing large compressive stresses on MnZn ferrite causes several negative effects to magnetic performance including lower permeability, lower saturation flux, and increased hysteresis loss. In [6], a compressive stress of 53.36 MPa increased the loss in a MnZn ferrite at 100 kHz, 100 mT, and 100°C by around 400% compared to when no compressive stress was applied. This effect has also been shown to decrease the permeability [6] and inductance [7] of ferrite core transformers. Therefore, this work models the compressive stress on ferrite caused by encapsulating material in inductive power transfer coil assemblies and experimentally validates the effect by measuring the losses in a small-scale coil assembly before and after an encapsulant is applied. The effect in a high power IPT prototype with inductive coil assemblies cured with a hard epoxy encapsulant is also shown with experimental measurements that are compared to a second prototype using a softer encapsulant.

II. ENCAPSULANT MATERIAL AND RESIDUAL STRESS

Residual stresses caused by encapsulation are caused by two primary mechanisms: chemical shrinkage and the differences in the thermal expansion coefficients of the ferrite and encapsulant. The first of these, chemical shrinkage, occurs when encapsulants cure. Many neat or unfilled epoxies shrink 1% to 5% when cured, while some ceramic-filled epoxies such as Aremco-Bond 2315 epoxy shrink less. The stress $\sigma_{shr,s}$ caused by the cure shrinkage S is [9]

$$\sigma_{shr,s} = S\left(\frac{E_f}{1+\frac{\phi_f}{\phi_e}\frac{E_f}{E_e}}\right). \quad (1)$$

which is a function of the volume ratios, ϕ_e and ϕ_f, and Young's moduli, E_e and E_f, of the encapsulant and ferrite, respectively.

The second effect is residual stress caused by curing at high temperatures followed by cooling. When cooling, differences in thermal expansion coefficients cause the encapsulant to shrink more than the ferrite. The ferrite is a metal-oxide ceramic with a relatively small thermal expansion coefficient. The stress due to this effect is

$$\sigma_{shr,c} = (\alpha_e - \alpha_f)(T - T_{cure})\left(\frac{E_f}{1+\frac{\phi_f}{\phi_e}\frac{E_f}{E_e}}\right). \quad (2)$$

Similar to the cure shrinkage, the stress is induced by the difference in thermal expansion coefficient, α_e and α_f, at a temperature T when cured at T_{cure} is [9].

The room temperature stress on ferrite caused by encapsulation in the silicone elastomer Cooltherm SC-320 and the ceramic-filled epoxy Aremco-Bond 2315 when cured at 120°C are shown in Fig. I. Both material manufacturers specify this curing temperature as an option. Here, the differences in thermal expansion coefficients and the high Young's moduli of the ferrite, Aremco 2315, and aluminum result in large stresses in

the ferrite. Aluminum is included as the ferrite may be tightly bonded to the aluminum by the encapsulant and the difference in its thermal expansion coefficient relative to the ferrite adds to the total stress on the ferrite. This represents the upper bound for aluminum with encapsulants with high adhesive strength and hardness such as the Aremco-Bond 2315 epoxy. The cured mechanical properties of the two encapsulants are compared with ferrite and aluminum in Table I. The Young's moduli for the encapsulants are extrapolated from the datasheet hardness values [10].

III. Validation with a Small-Scale Coil Assembly

To isolate the presence of higher ferrite losses caused by compressive stress, a small-scale coil assembly seen in Fig. 2 was made in order to compare losses with and without Aremco-Bond 2315 epoxy encapsulant. The assembly was comprised of an aluminum block with a milled cavity, a bottom layer of 2.7 mm Ferroxcube 3C95 ferrite, a 5 mm thick coil made of 8-turns of 10 AWG Litz wire with 38 AWG strands, and a top layer of 5 mm Ferroxcube 3C95 ferrite attached to an aluminum sheet held in place by bars of FR4. A notch was cut into the 5 mm ferrite to allow the passage of the coil leads such that the coil lays flat. The top 5 mm ferrite layer decreases the reluctance of the assembly so that higher flux is generated per unit current, increasing the hysteresis to wire loss ratio.

To cure the assembly, the following process was used: A thin layer of Aremco-Bond 2315 was poured and spread on the aluminum to adhere the ferrite to the aluminum, the 2.7 mm ferrite tiles were placed, an epoxy layer was poured to cover the 2.7 mm ferrite, the top 5 mm layer bonded to a thin aluminum sheet and the coil was placed in the cavity, the FR4 bars were fastened in place with nylon bolts, and finally the assembly was cured at 120°C for 6 hours.

Finite-element analysis (FEA) simulations were performed to estimate the compressive stress, flux density, and ferrite loss of the coil assembly. At 20 Arms in the 8-turn coil, a peak flux-density of 225 mT in the 2.7 mm layer of ferrite was predicted as in Fig. 3a. The mechanical simulation predicted a ferrite stress of 50-100 MPa in the 2.7 mm layer of ferrite as in Fig. 3b.

Loss measurements were taken with a WT1800 Yokogawa power analyzer and an AETechron 7794 power amplifier at the resonant point of a series tank comprised of the coil assembly and film capacitors. Different resonant frequencies were achieved by varying the number of capacitors in series. Slightly different frequencies were also measured to evaluate the effect of the shift of the resonant point from the decrease of the self-inductance.

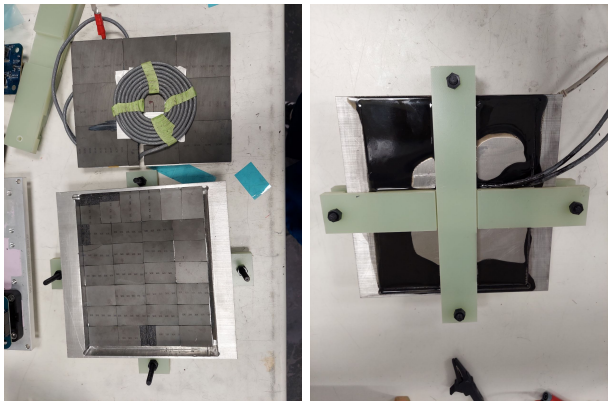

(a) (b)

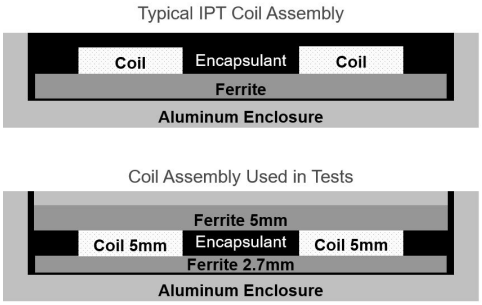

(c)

Fig. 2. The coil assembly used to verify the compressive stress effect of the Aremco-Bond 2315 epoxy on the ferrite hysteresis loss. (a) Top and bottom parts of the assembly. (b) The cured assembly. (c) Diagram of a typical IPT coil assembly and the small-scale coil assembly of this work.

As seen in Fig. 4a, the self-inductance decreased after curing from around 27.2 µH to 22.2 µH. With an airgap of 5 mm, this decrease may be from a drop in the magnetic permeability of the ferrite from stress [6]. The self-inductance of the coil directly relates the self-flux of the coil Φ through its turns N and the coil current I,

$$L = N\Phi/I. \tag{3}$$

With the drop in self-inductance, there is less flux in the ferrite per unit of current, potentially decreasing the core loss as a function of current. Hysteresis loss in ferrite is commonly modeled by the Steinmetz equation,

$$P_{fe} = C_m f^{\alpha} B_p^{\beta}. \tag{4}$$

Here, f is the frequency of the sinusoidal waveform and B_p is the peak magnetic flux density. The constants C_m, α, and β are calculated by curve fits of the measured loss over different frequencies and flux densities. Therefore, for loss measurements measured at the same current and frequency, the difference can be estimated by the $\beta = 2.44$ term of the 3C95 ferrite as in

$$\frac{P_{norm}}{P_{meas}} \propto \left(\frac{B_{p,norm}}{B_{p,meas}}\right)^{\beta} \propto \left(\frac{L_{cured}}{L_{uncured}}\right)^{\beta}. \tag{5}$$

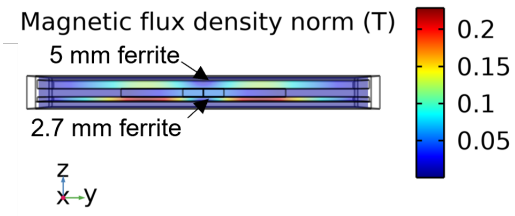

(a)

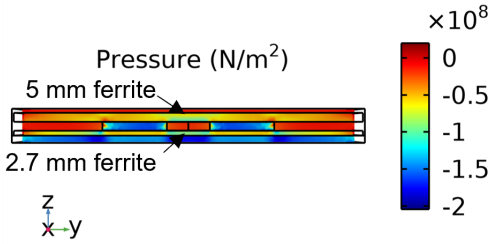

(b)

Fig. 3. FEA simulation of the small-scale coil. (a) Peak flux density in the coil with 20 Arms of coil current. (b) Stresses induced by thermal contraction of the materials from 120°C to 20°C.

Since the cured inductance is less than the uncured inductance, (5) predicts a decrease in the hysteresis loss of 64%. However, as seen in Figs. 4b and 4c, the tank losses approximately double for the cured coil relative to the uncured coil. The loss from the coil and capacitor resistance, R_{coil} and R_{cap} respectively, from the measured low-amplitude resistance as in Fig. 4a for the coil can be subtracted to estimate the loss of the ferrite alone as in

$$P_{fer} = P_{meas} - (R_{coil} + R_{cap})I^2. \tag{6}$$

In Fig. 5, with the loss of the wire and capacitor resistances taken into account, the cured ferrite loss is almost three times higher and almost five times higher when the effect of the decrease in self-inductance is accounted for. This result demonstrates the negative impact of a large compressive stress caused by a hard encapsulant in a coil assembly cured at high temperature. Similar to the result of [6], the hysteresis loss of the ferrite is estimated to be almost five-times higher due to the effect of stress simulated to be around 50-100 MPa in the 2.7 mm bottom layer of ferrite.

IV. Validation on Inductive Power Transfer Prototypes

A. Gen. 1 IPT Prototype

As detailed in [1], the first generation, or Gen. 1, of an inductive power transfer prototype was constructed with Aremco-Bond 2315 epoxy as the encapsulant of two identical coil assemblies as the ground assembly (GA) and vehicle assembly (VA). Overall, each coil assembly consists of a polycarbonate cover/coil former, a litz wire coil, a layer of ferrite, an aluminum enclosure, copper tubing to provide liquid cooling to the enclosure, and two capacitor banks. The thickness of the Ferroxcube 3C95 ferrite was 5 mm in the outer regions of the coil assembly and 10 mm in the inner region. This was done to reduce the ferrite flux density of the bipolar coil geometry in the center where it is concentrated.

An overview of the coil assembly construction is given in Fig. 7a. The layout of the ferrite tiles is shown in Fig. 7b. The ferrite tiles were test fit and numbered to match the tolerances of the tiles and ensure all pieces would fit before applying the encapsulant. With the ferrite ordered and removed, a thin layer of epoxy was poured on the aluminum and the ferrite tiles were placed on top according to their numbered positions. This was cured and then a second pour of the epoxy to bond the wire and coil former to the ferrite layer was performed and cured. Each cure of the encapsulant was 6 hours at 120°C in a large oven. In each use of the epoxy, the resin and hardener parts were mixed and then degassed in a vacuum chamber to eliminate air bubbles before pouring.

The wire and encapsulant layer have a 1 cm thickness, the ferrite layer has a 1 cm thickness in the inner region and 5 mm in the outer region, and the aluminum enclosure has a thickness of approximately 1 cm in the inner region and 1.5 cm in the outer region. The ferrite to encapsulant ratio is 1 in the inner region and 0.5 in the outer region and the ferrite to aluminum ratio is 1 in the inner region and 0.33 in the outer region. This leads to around 25 MPa stress from the encapsulant in the inner region and 50 MPa in the outer region and around 50 MPa from the aluminum in the inner region and around 75 MPa in the outer region from the one-dimensional model as in Fig. I. The ferrite, Aremco-Bond 2315, and aluminum all have high Young's moduli such that small strains caused by different thermal expansion coefficients cause large stresses in the materials when cured at high temperature. A simplified thermo-mechanical FEA simulation as in Fig. 6 also predicted the development of large mechanical stresses of around 40-60 MPa in the ferrite. This stress will degrade the magnetic performance of the ferrite as seen in the small-scale coil assembly.

Other elements of the Gen. 1 ferrite layout also contributed to increase the loss of the ferrite. The use of discrete ferrite tiles places many small air gaps within the ferrite sheet. Depending on the location of these gaps, localized concentrations of flux may occur possibly causing hot spots within the ferrite. As discussed in [5], for rectangular tiles or bars of ferrite, these concentrations are avoided by limiting the number of "T" intersections, where the corners of two tiles face the long side of a third tile due to offset and instead using "cross" intersection with four corners with all the tiles aligned. The authors

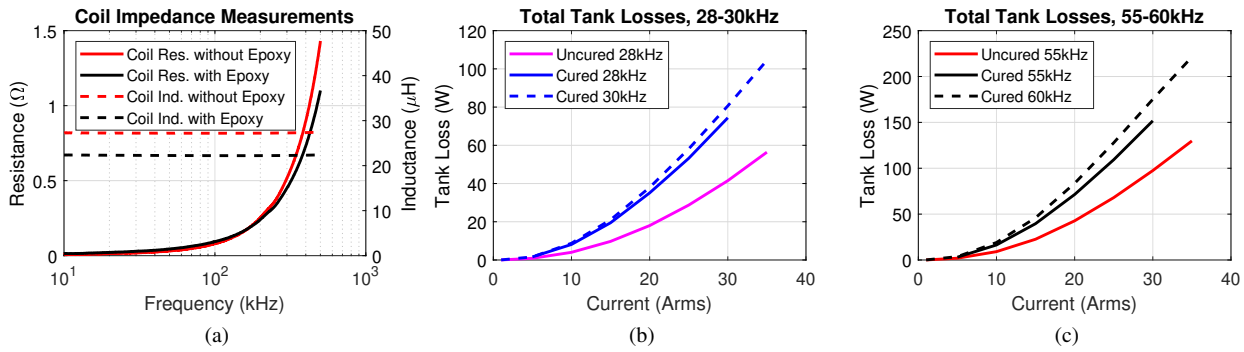

Fig. 4. Measurements of impedance and loss of the small-scale coil. (a) Impedance measurements of the coil before and after curing with epoxy. (b) Tank losses before and after curing with epoxy with the 30 kHz tank. (c) Tank losses before and after curing with epoxy with the 60 kHz tank.

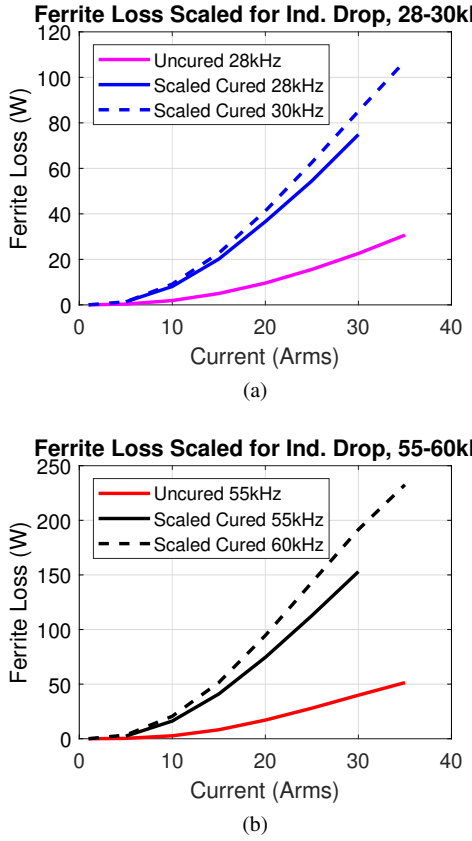

Fig. 5. Estimated ferrite loss without the loss from the measured tank resistance loss (6) and scaled for the drop in inductance (5) with the (a) 30 kHz and (b) 60 kHz tank.

also suggest to limit the number of cut tiles with non-machined irregular edges. In the Gen. 1 ferrite layout, there were several "T" intersection and thus locations for flux concentrations to form.

Also, in the Gen. 1 prototype the leads of the coil pass through openings in the aluminum enclosure and ferrite from the front side to the backside of the aluminum enclosure where the compensation capacitors are mounted. Routing the wire in this manner reduces the need for additional coil area outside the ferrite to route the wires and minimizes the high-frequency conductor length. However, this requires a opening or passthrough in the ferrite sheet which may lead to flux concentrations and higher overall ferrite loss than in an unbroken ferrite layer of the same thickness. Additionally, if the net current passing through each opening is non-zero, the ferrite sheet provides a low-reluctance path for circulating flux to form around the passthroughs in the plane of the ferrite as in Fig. 8. As also discussed in [5], this flux does not contribute to the coupling of the coils and results in additional ferrite loss.

The Gen. 1 GA and VA were tested up to 91.8 kW output power over a variety of loading conditions and misalignments. For the aligned[1] condition with near-unity gain with constant output resistance, the test results are plotted in Fig. 9. In Fig. 9a, the efficiency of each stage is shown. In these measurements, phase compensation of the high-frequency current probes was not performed, which led to some inaccuracy of the power factor, AC power, and efficiency measurement of the stages, but the overall DC/DC efficiency was not affected by the phase error of the current probes.

At low power levels, the coil-coil efficiency was high, matching the low-amplitude measurements of resistance and impedance of the Gen. 1 GA and VA. However, at high power levels, there was a rapid drop-off in coil-coil efficiency. At higher power levels, the coil-coil efficiency plot has perturbations in efficiency due to pulsed measurements and the effect of temperature on the coil efficiency. Measurements after a short resting time led to slightly higher efficiencies. Higher temperature operation, closer to the curing temperature of the

[1]After analyzing the data, it later was measured that the grid used to align the coil was off by around -7 mm in the X-direction and 5 mm in the Y-direction such that the actual test alignment was off in those directions.

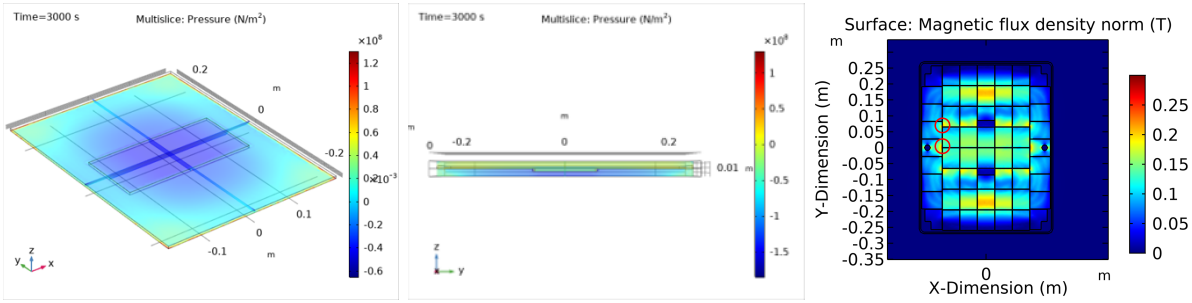

(a) (b) (c)

Fig. 6. FEA simulations the 120 kW prototype. (a) Isometric view of the resultant stress in the middle of the ferrite sheet caused by the aluminum and Aremco-Bond 2315 epoxy from a 120°C cure. (b) Side view of the stress simulation output. Here, the aluminum is below the ferrite and the epoxy is above. The double layer of ferrite of 10 mm thickness in the middle of the coil is shown in the middle region, the rest of the ferrite has a thickness of 5 mm. (c) The peak flux density of the ferrite at 2.5 mm with 164 A(rms) coil current. Here, two "T" intersections are labeled with red circles to highlight the flux concentrations in those areas.

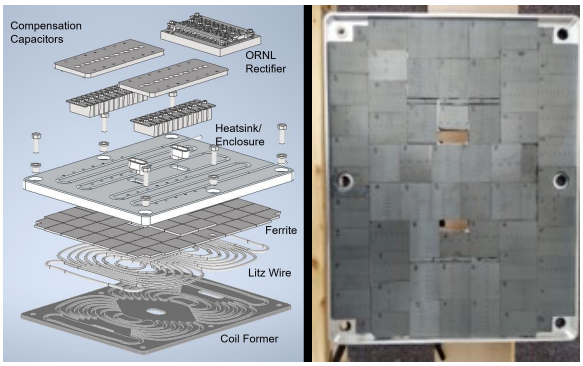

(a) (b)

(c)

Fig. 7. Construction of the Gen. 1 120 kW coil assemblies. (a) CAD layout of the coil assemblies. (b) Ferrite layout and numbering. (c) Cured coil assembly.

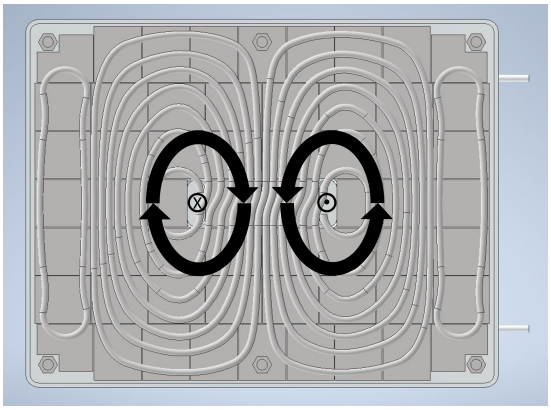

Fig. 8. The formation of circulating flux in the Gen. 1 ferrite sheet from two separate lead currents entering and leaving through separate passthroughs.

epoxy, reduces the thermal expansions stress (2) on the ferrite and decreases ferrite loss. From the material datasheet, higher ferrite temperatures up to around 100°C for Ferroxcube 3C95 will also reduce ferrite loss. The measured temperature during a few of these higher power test points up to 91.8 kW are plotted in Fig. 9b. These measurement were taken during power transfer with the fiber-optic thermometer Omega FOB100 which is impervious to interference from the magnetic fields of the IPT system. In the temperature measurements, the wire temperatures continued to increase after the system was turned off for a short period of time, suggesting that the ferrite temperature was higher than the wire.

The measured efficiency is much lower than expected from the low-amplitude impedance measurements of the coil assemblies. In Table II, the modeled DC/DC efficiencies at different alignments and power levels are compared to the measured values. These models calculate the ferrite loss from the Steinmetz coefficients directly from the datasheet values without including non-ideal ferrite loss mechanisms as previously discussed. As seen, the measured losses are around twice the modeled values. This matches the behavior of a ferrite loss that is significantly higher than expected similar to that seen in the small-scale coil assembly. This points to elevated ferrite loss caused by the compressive stresses in the ferrite, non-ideal ferrite tile layout, and the circulating flux from the separate passthrough of the leads through the ferrite sheet to the backside of the enclosure.

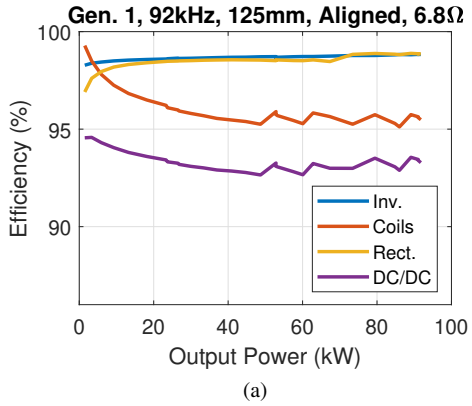

Fig. 9. Measurements of the coil assembly at alignment[1] and a 125 mm airgap. (a) Efficiency breakdown up to 91.8 kW output power. (b) Thermal measurements of the system during testing points around 91.8 kW.

Table II
SUMMARY OF THE MEASURED AND MODELED DC/DC EFFICIENCY OF THE GEN. 1 SYSTEM AT DIFFERENT ALIGNMENTS[1] AT AN AIRGAP OF 125 MM.

Alignment (X,Y)	DC Output Resistance	Power Level	Meas. DC/DC Eff.	Model DC/DC Eff.
(0cm, 0cm)	6.8 Ω	91.8 kW	93.3%	96.3%
(5cm, 0cm)	5.9 Ω	48.5 kW	93.3%	96.2%
(10cm, 0cm)	5.5 Ω	46.7 kW	91.8%	95.3%
(0cm, 5cm)	5.5 Ω	44.2 kW	92.1%	95.2%

B. Gen. 2 IPT Prototype

To validate that modifying the coil construction and encapsulant reduces these losses, Generation 2 (Gen. 2) coil assemblies were made with a soft and room temperature curing Cooltherm SC-320 silicone elastomer encapsulant as in Table I, a simplified ferrite layout, and a single passthrough for the leads to the backside of the enclosure as in Fig. 10. The measured impedance and tank loss of the Gen. 1 and Gen. 2 GAs are compared in Fig. 11. Here the self-inductance of the Gen. 2 GA is larger than the Gen. 1 GA, possibly due to the drop in

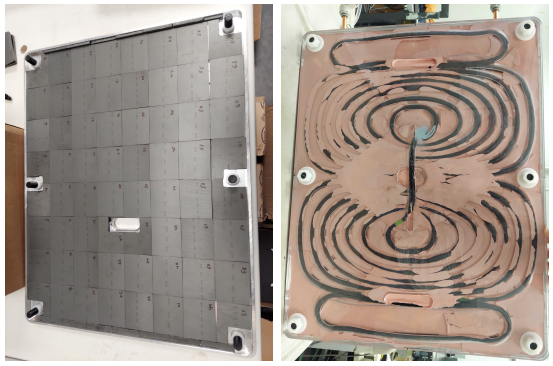

(a) (b)

Fig. 10. Construction of the Gen. 2 120 kW coil assemblies. (a) Ferrite layout and numbering of one of the Gen. 2 coil assemblies. (b) Frontside of a cured Gen. 2 coil.

Table III
SUMMARY OF THE DC/DC EFFICIENCY OF THE GEN. 2 SYSTEM NEAR UNITY GAIN AT DIFFERENT ALIGNMENTS[1] AT AN AIRGAP OF 125 MM.

Alignment (X,Y)	DC Output Resistance	Power Level	Meas. DC/DC Eff.	Model DC/DC Eff.
(0cm, 0cm)	5.9 Ω	120.4 kW	96.6%	96.7%
(5cm, 0cm)	5.9 Ω	64.2 kW	96.6%	96.8%
(10cm, 0cm)	5.9 Ω	52.7 kW	95.9%	96.0%
(0cm, 5cm)	5.0 Ω	51.2 kW	96.1%	96.2%
(10cm, 5cm)	4.1 Ω	51.7 kW	95.2%	95.1%

self-inductance from the stress of the encapsulant in the Gen. 1 GA. The tank loss measurements were made with a power analyzer with a series tank of each of the GAs with current from a power amplifier near the resonant frequency of the tanks. The same capacitor bank and leads were used for both series of measurements.

As seen in Fig. 11a, the low-amplitude resistances of the coil assemblies are nearly identical, but high-amplitude measurements in Fig. 11b show a large difference in the losses of the coil assemblies. Using the same inverter and compensation elements as with the Gen. 1 system, the measured efficiency of the Gen. 2 system is higher. At alignment[1] at a 125 mm airgap, a 96.6% DC/DC efficiency was measured at 120.4 kW as in Fig. 11c. Phase compensation on the power analyzer current probes in this measurement led to a more-accurate efficiency breakdown. Here, the measured coil-coil efficiency decreases as power level increases, but not to the extent as the Gen. 1 system. The efficiency measurements, as summarized in Table III, match the modeled values much more closely than in the Gen. 1 system and no large excess loss beyond that predicted by the material Steinmetz parameters was observed. More details and measurement results are detailed in [1].

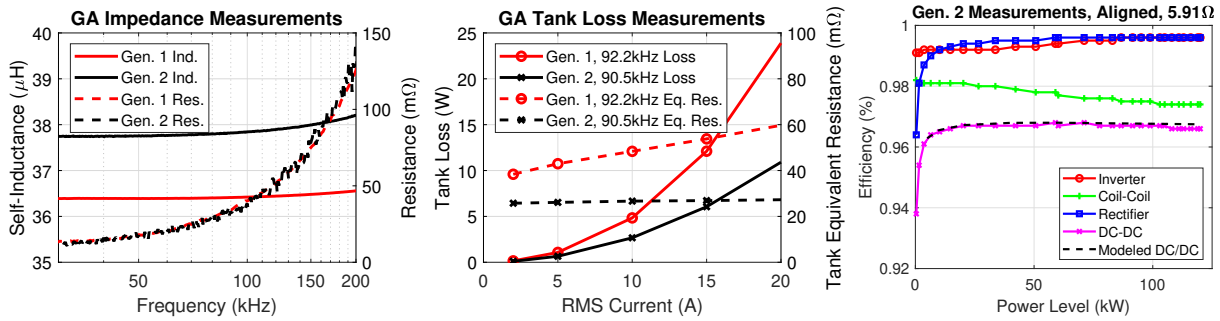

Fig. 11. Comparison of tank measurements of the Gen. 1 and Gen. 2 GAs. (a) Self-inductance and resistance impedance analyzer measurements. (b) Power analyzer measurement of the tank loss of the Gen. 1 and Gen. 2 GAs at amplitude. Testing of the Gen. 2 system at alignment[1] and 125 mm. (c) Measured efficiency breakdown vs. output power.

V. Conclusion

The encapsulation of IPT coil assemblies using hard materials with high curing temperatures can cause large residual mechanical stress due to differences in thermal expansion and cure shrinkage. These stresses cause higher hysteresis loss and decreased magnetic permeability in MnZn ferrite. In this work, the effect is demonstrated in a small-scale cured coil assembly encapsulated with a hard, thermally conductive epoxy that causes three to five times higher ferrite loss. Furthermore, a high-power prototype inductive power transfer system cured with the same epoxy demonstrates a rapidly decreasing coil-coil efficiency. It is postulated that some of this excess loss is caused by the encapsulant stress on the ferrite, a non-ideal ferrite tile layout, and separate passthroughs of the coil leads through the ferrite. A second version of this prototype with these issues fixed results in higher coil-coil efficiency and overall DC/DC efficiency.

Therefore, care must be taken in selecting the encapsulant of IPT coil assemblies to avoid large residual stresses on ferrite. Although hard and thermally robust epoxies with quick curing times at high temperatures may be beneficial for mechanical strength and adhesion, the large stresses they can generate may cause excessive ferrite loss in the coil assemblies.

Acknowledgements

The authors would like to thank Chuhee Lee and Hendrik Mainka for their mentorship in the project.

References

[1] A. Foote, "Fourier analysis and optimization of inductive wireless power transfer for electric vehicle charging," Ph.D. dissertation, University of Tennessee, 2023.

[2] B. Zhang, J. Deng, W. Wang, L. Li, Z. Wang, S. Wang, and G. Guidi, "Multi-objective thermal optimization based on improved analytical thermal models of a 30 kW IPT system for EVs," *IEEE Transactions on Transportation Electrification*, 2022.

[3] S. Zimmer, M. Helwig, P. Lucas, A. Winkler, and N. Modler, "Investigation of thermal effects in different lightweight constructions for vehicular wireless power transfer modules," *World Electric Vehicle Journal*, vol. 11, no. 4, p. 67, 2020.

[4] M. C. Kulan, S. Sahin, and N. J. Baker, "An overview of modern thermo-conductive materials for heat extraction in electrical machines," *IEEE Access*, vol. 8, pp. 212 114–212 129, 2020.

[5] P. A. J. Lawton, F. J. Lin, and G. A. Covic, "Magnetic design considerations for high-power wireless charging systems," *IEEE Transactions on Power Electronics*, vol. 37, no. 8, pp. 9972–9982, 2022.

[6] V. Tsakaloudi, D. Holz, and V. Zaspalis, "The effect of externally applied uniaxial compressive stress on the magnetic properties of power MnZn-ferrites," *Journal of Materials Science*, vol. 48, no. 10, pp. 3825–3833, 2013.

[7] W. J. Kirk, "Ferrite-core transformer bonding and potting. final report," *Bendix Corporation*, 1974. [Online]. Available: https://www.osti.gov/biblio/4307025

[8] Ferroxcube, "Soft ferrite: Ferrite materials survey," 2008. [Online]. Available: https://ferroxcube.home.pl/prod/assets/sfmatgra_frnt.pdf

[9] I. M. Daniel, O. Ishai, I. M. Daniel, and I. Daniel, *Engineering mechanics of composite materials*. Oxford University Press New York, 2006.

[10] K. Larson, "Can you estimate modulus from durometer hardness for silicones?" *Dow Corning Corporation*, 2016.